THE GROUND CALIBRATION OF THE BACK-SIDE ILLUMINATED CCD CAMERA OF X-RAY IMAGING SPECTROMETER (XIS) ONBOARD ASTRO-E2 (SUZAKU)

H. Yamaguchi[1], H. Nakajima[1], K. Koyama[1], T. G. Tsuru[1], H. Matsumoto[1], H. Tsunemi[2], K. Hayashida[2], K. Torii[2], M. Namiki[2], S. Katsuda[2], D. Matuura[2], and T. Miyauchi[2]

[1]Department of Physics, Graduate School of Science, Kyoto University, Sakyo-ku, Kyoto, Japan
[2]Department of Earth and Space Science, Graduate School of Science, Osaka University, Toyonaka, Osaka, Japan

ABSTRACT

We report on the results of the ground calibration of the back-side illuminated (BI) Charge-Coupled Device (CCD) onboard Suzaku(Astro-E2). The BI CCD has higher quantum efficiency (QE) below $\sim$4 keV than Front-side illuminated (FI) CCDs. By chemisorption charging process, furthermore, the BI chip achieved very good energy resolution comparable to the FI chip. However, several problems were found by our ground calibration. One of them is charge trailing, and we corrected this phenomenon by a newly developed method, "Charge Trail Correction". Another problem is that the constant split threshold, a key parameter for the Grade method, gives a poor performance for the BI chip. Thus we introduced a new Grade method with a variable split threshold depending on the incident X-ray energy.
Analyzing the ground calibration data with these new methods, we built the response function of BI CCD.

Key words: Suzaku, XIS, X-ray CCD, calibration.

1. INTRODUCTION

Suzaku was launched from Uchinoura Space Center (USC) on 10 July 2005 as the Japanese fifth X-ray astronomical satellite, and successfully put into the orbit. Unfortunately, X-Ray Spectrometer (XRS; Mitsuda et al. (2001)), one of the main instruments of Suzaku, became not operational because of helium loss, but all of the other detectors, Hard X-ray Detector (HXD; Makishima et al. (2001)) and XISs, are still working properly. The HXD consists of phoswitch crystal scintillators (GSO/BGO) and PIN silicon solid-state detectors. It has a large energy range of 10–600 keV band, and the sensitivity is higher than any other hard X-ray detectors especially in the 10–200 keV band. XISs are composed of four sensors, which are placed at the focal plane of four X-Ray Telescopes (XRTs). Three of them are the FI CCDs (XIS0, XIS2, XIS3), and the other is the BI CCD (XIS1). We will describe the BI CCD in detail in the following section.

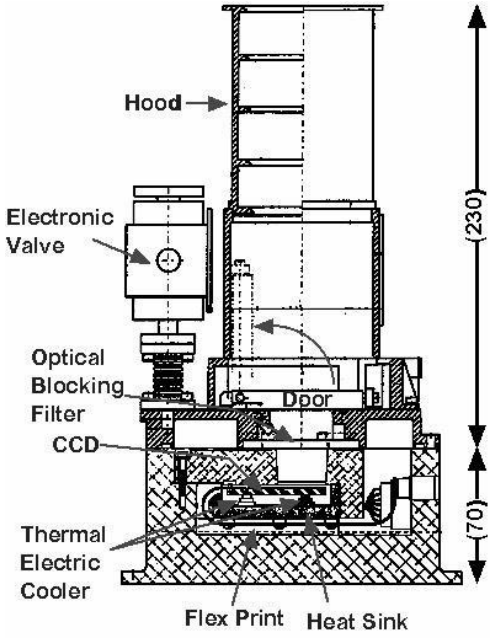

Figure 1. Schematic view of XIS sensor component.

Figure 1 shows the schematic view of one XIS sensor. Each sensor has a single CCD chip with an imaging area of 1024 $\times$ 1024 pixels. The pixel size is 24 μm $\times$ 24 μm. The field of view and the time resolution (readout time) are $18' \times 18'$ and 8 sec, respectively. The CCD chip is cooled into -90 °C by Thermo-Electric Cooler (TEC) which is controlled by Thermal Controller Electronics (TCE). The chip has four readout nodes and each node reads the signals from 256 columns of the chip, and then these divided regions of the chip are called as Segment A–D. The analog signals from the sensor are transferred to the Analog Electronics (AE) and converted into the digital signals. Then they are sent to the Digital Electronics (DE) and X-ray events are extracted.

All XISs are developed by the collaboration of Massachusetts Institute of Technology (MIT), Japan Aerospace Exploration Agency (JAXA)/Institute of Space and Astronautical Science (ISAS), Kyoto University, Osaka University, Rikkyo University, Ehime University, Kogakuin University, and RIKEN (The Institute of Physical and Chemical Research).

2. DESCRIPTION OF XIS/BI

In the history of Japanese X-ray astronomy, Suzaku is the first satellite which introduces BI CCD. Since there are no gate structure obstructing incident X-rays on the surface of the BI CCD, it has high quantum efficiency (QE) for soft X-rays. Figure 2 shows the QE of FI and BI CCD, which was modeled on the results of our ground calibration. We can see that the BI CCD has much higher QE below $\sim$3.5 keV than the FI CCD. However, because the depletion layer of BI CCD is thinner than that of FI CCD (~ 75 μm and ~ 45 μm for FI and BI, respectively), the QE of BI CCD for hard X-rays is lower than that of FI CCD.

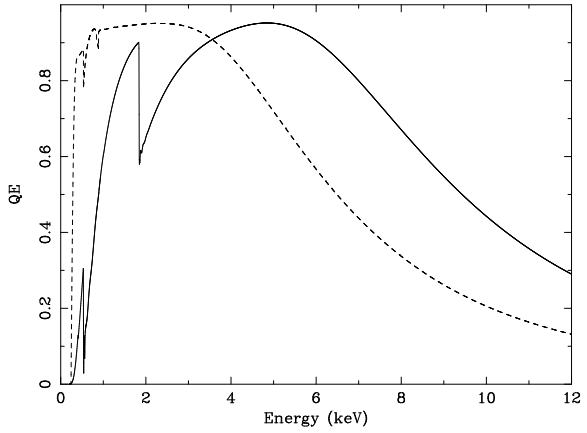

Figure 2. Quantum efficiency of FI CCD (solid line) and BI CCD (dash line).

Generally, the charge collection efficiency of BI CCD is poorer than that of FI CCD. Therefore the energy resolution of BI CCD tends to become worse. For example, the energy resolution of Advanced CCD Imaging Spectrometer (ACIS)/BI loaded into Chandra (Weisskopf et al. (2002)) was about two times worse than that of FI devices, even before the launch. The XIS/BI is improved in this problem. Figure 3 shows the structure of the XIS/BI chip. In the chemisorption charging process, the back surface of the wafer is first oxidized. The resulting oxide layer is then coated with a very thin layer of silver. The silver catalyzes dissociation of molecular oxygen on the surface during processing, leaving fixed, negatively charged oxygen atoms on the surface. Then the electric field between the surface and electrode is strengthened, and the collection efficiency of photo-electrons is improved.

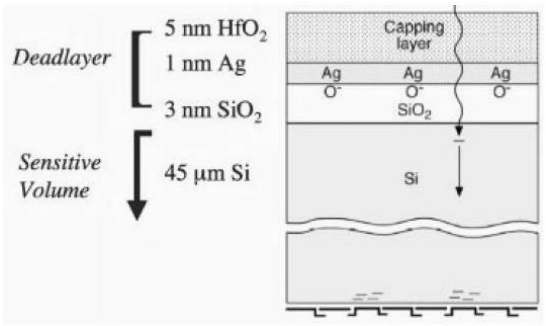

Figure 3. Schematic of the XIS/BI chip treated with the chemisorption charging process.

3. GROUND CALIBRATION

3.1. Overview of the Calibration

The CCD calibration task was shared with MIT, Osaka University, Kyoto University, and JAXA/ISAS. After the simple chip level calibration at MIT, the detailed wide band calibration combined with flight AE was done by Osaka University and Kyoto University. Osaka University group investigated the low energy ($<$ 2 keV) X-ray response of the sensor using grating spectrometers. On the other hand, Kyoto University made investigation into the high energy ($>$ 1.5 keV) response with fluorescence X-rays from the targets (Al, Cl, Ti, Fe, Zn, Se) and from the ^{55}Fe source.

3.2. Event Detection

For FI CCD data, we use the ASCA Grade method (see Figure 4) to detect X-ray events. In the case of XIS, we consider that most of the X-ray events don't split into a region larger than 2$\times$2 pixels, and we then regard the events of Grade 0, 2, 3, 4, and 6 as the X-ray events. On the other hand, all of the events which split over the 2$\times$2 pixels region are classified into Grade 7 and regarded as background events, because they are usually formed by the cosmic-ray. Here, the split threshold is the very important parameter for the Grade method, because the energy resolution and detection efficiency are very sensitive to the split threshold. For the XIS/FI, it is optimized to 20 ADU.

We also analyzed the BI data using the Grade method with the same split threshold to FI. Our calibration data shows, however, the imperfection of the original Grade method for the analysis of BI CCD.

3.3. Charge Trailing

First, we found peculiar non-uniformity of Grade branching ratio. Figure 5 shows the distributions of Grade 0 and

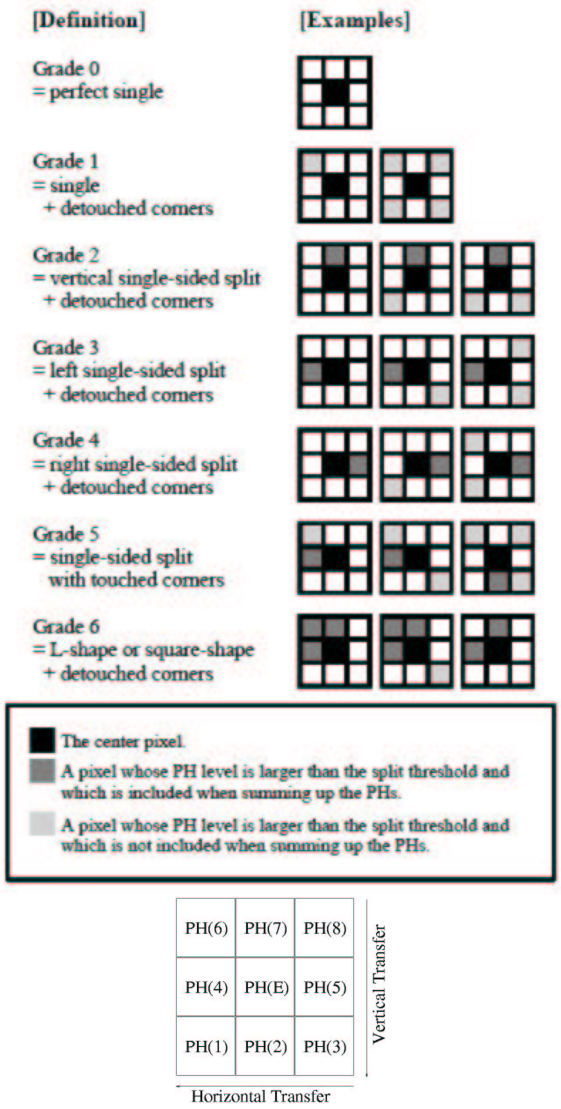

Figure 4. Top:Classification of ASCA Grade., Bottom:Definition of pixel name surrounding the center pixel of event (PH(E)).

Grade 2 events when the BI CCD was illuminated uniformly by X-rays of 8.6 keV. We can see that the event number of Grade 0 decreases with the number of vertical transfers in the imaging area. On the other hand, the event number of Grade 2 increases with the vertical transfer. Grade 2 events include two patterns.; the events split into PH(2) (see Figure 4 bottom) and split into PH(7), and only the latter contributes the increasing of the Grade 2 counts with the vertical transfer. This fact suggests a part of the charge of each event trails to a pixel opposite to the direction of the vertical transfer, and the amount of trailing charge increases in the charge transfer process. Similarly, some events which spread more widely, for example Grade 6 events, become Grade 7 by the charge trailing. As a result, these events which should be detected as X-ray events are classified into background events and abandoned. This phenomenon causes the reduction of the detection efficiency. We therefore must quantify this effect and properly correct it.

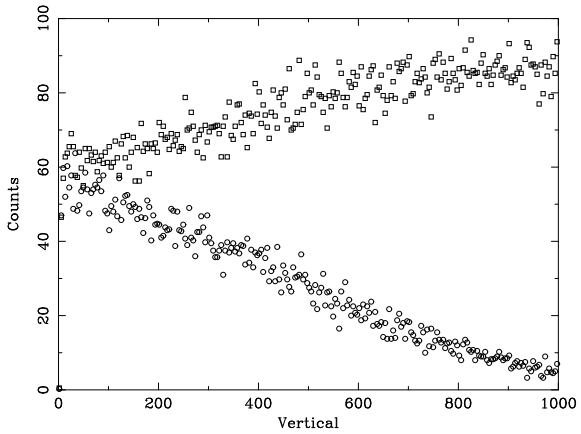

Figure 5. Event number distributions of Grade 0 (circle) and Grade 2 (square). "Vertical" means the number of the vertical transfer in the imaging area.

We estimated the probability of charge trailing. The left of Figure 6 shows the correlation between the number of vertical transfers and the pulse height of PH(7) (shown as Q') extracted from Mn-Kα events. Then we found Q' was proportional to the number of vertical transfers, and coefficient (C) was obtained as 6.3×10^{-3} by fitting with linear function. Here, we define the probability of charge trailing per pixel transfer as "Charge Trail Ratio", CTR. Then we can approximately estimate CTR with the equation;

$$\mathrm{CTR}\ [1/\mathrm{Transfer}] = C/Q, \qquad (1)$$

where Q means the mean pulse height of the noticed events. For Mn-Kα events, Q is $\sim$1503 and CTR is estimated as 4.5×10^{-6}.

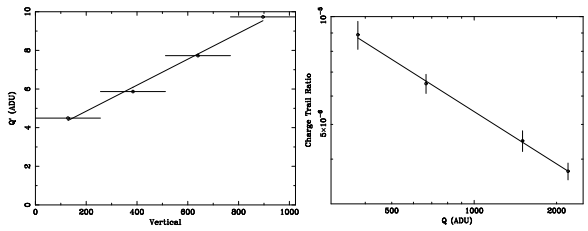

Figure 6. Left: Correlation between the number of the vertical transfer and the amount of the trailing charge. Q' means the pulse height of PH(7)., Right: The pulse height dependence of Charge Trail Ratio, CTR.

Furthermore, we found that CTR also depends on the energy of incident X-rays. We estimated CTR for Al-Kα events, Cl-Kα events, and Zn-Kα events, similarly to Mn-Kα events. Then the relation between the CTR and Q is given as the right of Figure 6, and it can be well fitted with the power-law model expressed as the solid line in the right of Figure 6. And the pulse height dependence of CTR is estimated as

$$\mathrm{CTR}\ [1/\mathrm{Transfer}] = (1.72 \times 10^{-4}) \times Q^{-0.5}. \qquad (2)$$

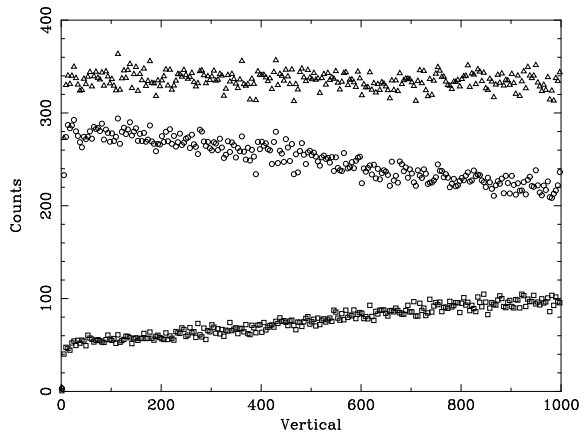

Figure 7. Event number distributions of Grade 0, 2, 3, 4, and 6 (circle) and Grade 7 (square) before Charge Trail Correction and Grade 0, 2, 3, 4,and 6 after the correction (triangle) when the CCD was illuminated uniformly by X-rays of 8.6 keV.

With this result, we have developed a new analysis method, "Charge Trail Correction". First, we estimate the amount of the trailing charge of each event with equation 2, and we then correct the pulse height of PH(E) and PH(7); remove the trailing charge from PH(7) and add it to PH(E). Figure 7 shows the distributions of detected events (Grade 0, 2, 3, 4, and 6) and Grade 7 events before the correction and detected events after the correction. This result means a lot of Grade 7 events due to charge trailing are successfully reduced by the correction, and the distribution of detected events becomes uniform. Then the detection efficiency of a whole chip successfully improved about 10–20 percent.

3.4. Split Threshold Optimization

The second problem was that we found much worse energy resolution than the theoretically expected value. Table 1 compares the energy resolution of XIS/BI with that of XIS/FI. Thanks to the chemisorption process, the energy resolution of BI for high energy X-rays is comparable to that of FI. However the energy resolution becomes worse as incident X-ray energy becomes lower.

Table 1. Energy resolution of BI and FI, and the ratio of them. Both of them are analyzed with split threshold of 20 ADU.

Ex (keV)	BI (eV)	FI (eV)	Ratio (BI/FI)
0.28	57.0	33.1	1.72
0.53	63.0	42.2	1.49
4.51	129.0	114.1	1.13
8.63	170.7	159.0	1.07

As far as we use the Grade method, the charge split into surrounding pixels is not summed up unless the pulse heights of these pixels exceed the split threshold. In other word, if the pulse heights of split pixels are lower than the split threshold, these split components are ignored, and the energy resolution becomes worth as a result. The fact that the energy resolution is much worse than the expected value means that the split threshold is too large to detect such split charge. Therefore, split threshold should be optimized to be able to detect such split charge enough. In the case of the BI chip, furthermore, low energy events which are produced at far from the electrode are spread more widely than high energy events. Therefore, the degradation of energy resolution compared with the FI is notable especially in low energy band.

We then optimized the split threshold for the BI CCD. The left of Figure 8 shows the energy resolution and QE as a function of split threshold, where only O-Kα events are used. Because of the reason mentioned above, the energy resolution becomes better as the split threshold becomes lower. However QE becomes lower, because the X-ray events classified as Grade 7 increase. Furthermore, the QE suddenly drop where the split threshold becomes lower than a certain value. We then determine the value which is a few ADU larger than those drop point as the split threshold. In the case of O-Kα events, we choose 10 ADU as the split threshold. Then, energy resolution becomes $\sim$55 eV which is better by $\sim$13% than when the split threshold is 20 ADU ($\sim$63 eV). In addition, QE is lower by only $\sim$2%. Therefore, we can conclude that 10 ADU is better than 20 ADU as the split threshold. For high energy events, however, we found that 10 ADU is too low as split threshold. The right of Figure 8 shows the same relation as the left of Figure 8, in the case of Zn-Kα events. We can see that the value where QE suddenly drops for Zn-Kα is larger than that of O-Kα. Therefore, if we choose 10 ADU as split threshold, the energy resolution becomes better by only $\sim$4%, but QE becomes lower by $\sim$6%. We then optimized the split threshold for Zn-Kα events independently, and 13 ADU was chosen.

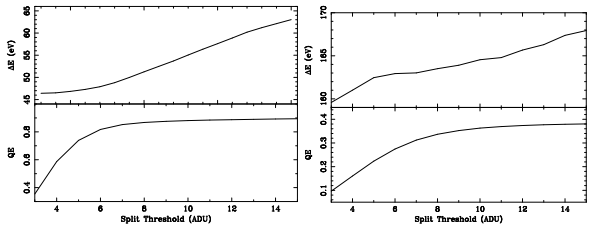

Figure 8. Left: The energy resolution (top) and QE (bottom) as a function of split threshold, where O-Kα events are used., Right: The same relation but Zn-Kα events are used.

We also optimized split threshold for other energy events and the results are shown in Figure 9. Because the optimum split threshold has energy dependence as shown in Figure 9, we decided to introduced a new Grade method with variable split threshold depending on the incident X-ray energy. The solid line in Figure 9 shows the best-fitted model for the relation between the optimum split

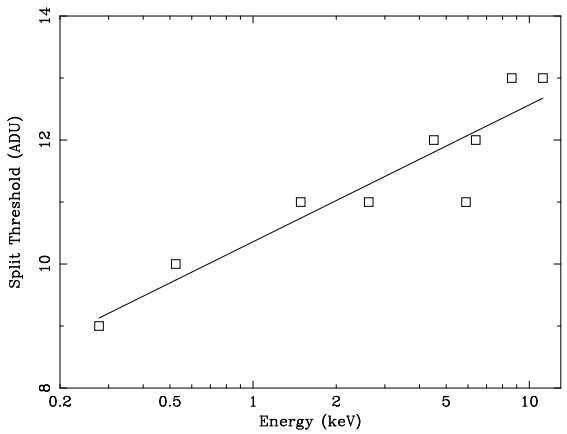

Figure 9. Variable split threshold for XIS/BI. The squares show the optimized split threshold at each energy, and solid line shows the best-fitted model.

threshold and X-ray energy. The function was given as

$$\mathrm{S\ [ADU]} = 10.36 + 2.208 \log_{10}(\mathrm{E\ [keV]}), \quad (3)$$

where S and E mean split threshold and X-ray energy, respectively. In the BI analysis, we make Grade classification using variable split threshold according to equation 3. Of cause, we don't know the incident X-ray energy before analysis. We therefore once estimate the energy with temporary split threshold, and decide new split threshold with equation 3, we then calculate summed pulse height of the event using new split threshold.

We analyzed the data using the new Grade method with variable split threshold and the energy resolution is given as shown in Figure 10. Good energy resolution comparable to FI is achieved in the whole energy band of 0.2–13keV with the new method.

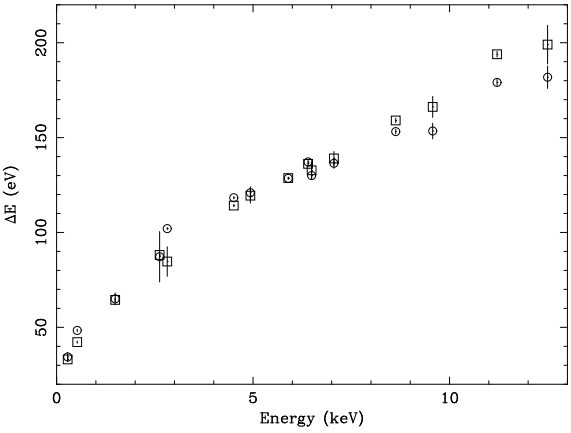

Figure 10. Energy resolution of BI (circle) and FI (square).

4. RESPONSE FUNCTION

Finally, we built the response function of XIS/BI using the ground calibration data analyzed with the new methods. Figure 11 shows the gain of BI CCD segment C. The relation between X-ray energy and pulse height is fitted with the linear function which has a break at the energy of Si-K edge (=1.838 keV). We then obtained the gain of 255.5 ch/keV for the energy band lower than 1.838 keV, and 255.2 keV for the energy band higher than 1.838 keV. The difference of the gain among the segments is less than 4%.

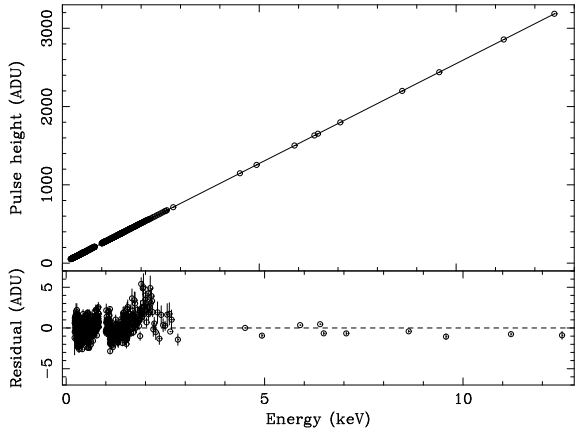

Figure 11. The energy scale linearity of XIS/BI.

In the case of XIS/BI, the response function is expressed with five component model; main peak, sub peak, Si-escape peak, Si peak, and constant. The ratio of the intensities of these components depend on X-ray energy. Therefore, we estimated the relation between these ratio and X-ray energy, and determined the line profile for whole energy band. Figure 12 shows the spectra of O-K and Mn-K obtained by our ground calibration, and they are well fitted with the response function we built.

The gain, energy resolution, and line profile will change gradually on the orbit. However, we have already prepared the analysis software which is able to adjust the changes of the performance. We will renew the response function periodically with onboard calibration data and provide it for all users.

5. SUMMARY

We have reported the results of the ground calibration of XIS/BI CCD. The BI CCD has high quantum efficiency for low energy X-rays, and very good energy resolution was achieved by chemisorption process. We developed the new method, Charge Trail Correction and the new Grade method with variable split threshold, and then we successfully brought out the performance of the BI CCD. We built the response function with the ground calibration data and prepared the analysis software.

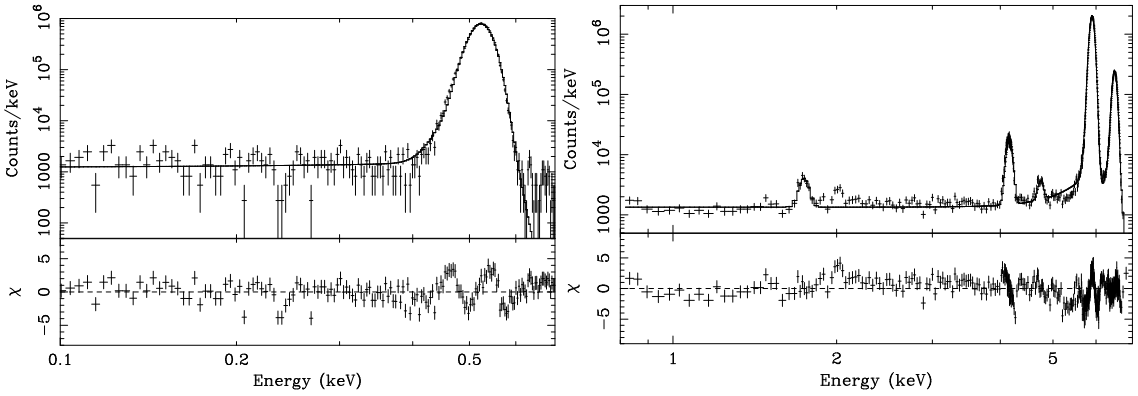

Figure 12. The XIS/BI spectrum of O-K line (left) and that of Mn-K line (right) fitted with response function built with the ground calibration data.

ACKNOWLEDGMENTS

We thank all of the members of XIS team. H. Y. and H. N. are supported by Japan Society for the Promotion of Science (JSPS) Research Fellowship for Young Scientist.

REFERENCES

Mitsuda, et al., ASP Conf. Ser. 251 (2001) 570

Makishima, et al., ASP Conf. Ser. 251 (2001) 564

Weisskopf, et al., Publ. Astron. Soc. Pacific 114 (2002) 1.